Analysis of a self-oscillating mixer based on a slow-wave structure

Mabel Pontón, Franco Ramírez, Sergio Sancho, Almudena Suárez

Universidad de Cantabria, Spain

{mabel.ponton, franco.ramirez, sergio.sancho, almudena.suarez}@unican.es

***Abstract* — This work presents a self-oscillating mixer (SOM) based on a slow-wave structure for phase-noise reduction. Emphasis is placed on the analysis/optimization methods, which include aspects such as conversion gain, nonlinear distortion, and operation boundaries. In a first stage, the parameters of the slow-wave structure are optimized to obtain a low phase-noise spectral density. As an example, a structure based on a unit cell containing a Schiffman section is considered. Then, the SOM behavior is addressed through an analytical model that should enable an understanding of its main operation characteristics. A practical FET-based circuit at 2.3 GHz is simulated with some novel harmonic-balance techniques and experimentally characterized.**

***Keywords* — Self-oscillating mixer, phase noise, stability, bifurcation.**

I. Introduction

Compact, low-cost, and low-consumption frontends are of paramount interest for sensor systems, imaging arrays and radio-frequency identification, among other. These needs have brought new attention [1]-[3] to self-oscillating mixers (SOMs), which enable an implementation of both the oscillation and mixing function in a single component [2]-[3]. Due to their active behaviour, they can also provide conversion gain. Their main drawback is the oscillation phase noise, which is basically up- or down-converted to the output signal [4]. To reduce this phase noise, we propose the use of a slow-wave structure, which should provide a high group delay in a compact size. In slow-wave structures, a low phase velocity is achieved by increasing the effective capacitance and/or inductance of the line, implemented in practice through different strategies [5]-[6]. In prior works, slow-wave structures have been used in free-running oscillators [6]-[7] but, to the best of our knowledge, they have not been considered yet for SOM design.

In a first stage, the parameters of the slow-wave structure are optimized to maximize its frequency selectivity and, thus, enable a low phase noise. As an example, a structure based on a unit cell containing a Schiffman section is considered [5]. Then, the SOM behavior is addressed through an analytical model that should enable an understanding of its main operation characteristics. In fact, the multi-function capability of SOMs comes at the expense of a more complex behavior in an autonomous quasi-periodic regime [8], delimited by two distinct bifurcation phenomena: the asynchronous extinction of the oscillation, or inverse Hopf bifurcation [9], and the injection locking by the input source. A practical FET-based circuit will be simulated with some novel harmonic-balance (HB) methods and experimentally characterized. Note that instead of achieving a record performance, the goal is to describe novel analysis/optimization methods for SOM based on slow-wave structures.

II. Free-Running Oscillator

A. Selection of the parameters of the slow-wave structure

To obtain a low phase noise oscillation, we have used a short-circuited slow-wave structure based on a unit cell containing a Schiffman section [5] [Fig. 1(a)], though the procedures could equally be applied when using other slow-wave configurations. The structure must resonate at the specified oscillation frequency with a high slope of the input susceptance $\partial B_s / \partial \omega$. In a first step, the susceptance is analysed at the desired oscillation frequency $\omega = \omega_o$ (2.3 GHz) to obtain its zeroes versus the length l [Fig. 2(a)], that is, the length values fulfilling $B(l_n) = 0$. In a second step, a frequency sweep is carried out for each l_n to evaluate $\partial B / \partial \omega$ [Fig. 2(b)]. A higher slope is obtained for a longer l at the expense of closer additional resonances. The selected value is l = 5.48 mm.

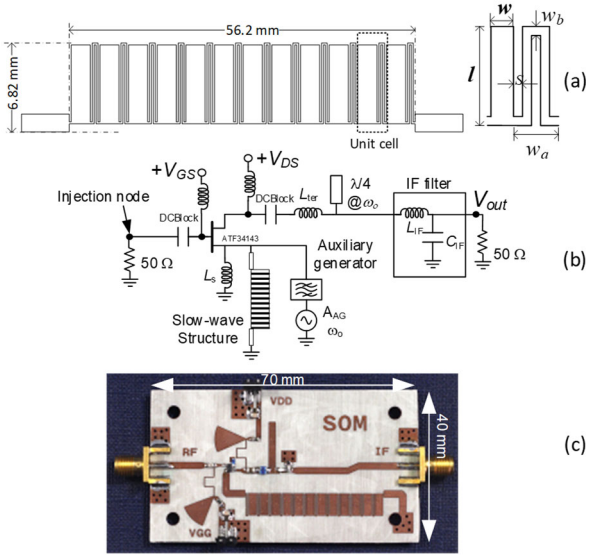

Fig. 1 (a) Slow-wave structure based on a unit cell containing a Schiffman section. (b) Proposed SOM. An auxiliary generator (AG) is connected to the source terminal for simulation purposes. (c) Prototype on Rogers 4003C.

B. Phase noise

In the oscillator design carried out here, the slow-wave structure is connected to the source terminal, as shown in Fig. 1. The output network contains a quarter-wave open-ended

transmission line at the oscillation frequency and a simple low-pass filter with the values L_{IF} = 10 nH and C_{IF} = 30 pF. Although the phase noise should be low due to the high susceptance slope, it can be further minimized in HB with the aid of an auxiliary generator (AG). This AG is connected to the source terminal [Fig. 1(a)], and operates at the desired oscillation frequency $\omega = \omega_o$. A sweep in l is carried out, optimizing the AG amplitude A_{AG} and the width w to obtain a zero value of the AG current-to-voltage ratio [$Y_{AG}(A_{AG}, w) = 0$]. At each step of the sweep, the phase noise is evaluated with the conversion-matrix approach. Fig. 3(a) presents the variation versus l of the spectral density at 100 kHz offset frequency from the carrier. Of course, the oscillation at $\omega = \omega_o$ may be impossible for some pairs l, w, which occurs in the shadowed region. Outside this region, there are two minima and the selected one corresponds to l = 5.62 mm and w = 2 mm, which will slightly reduce the size.

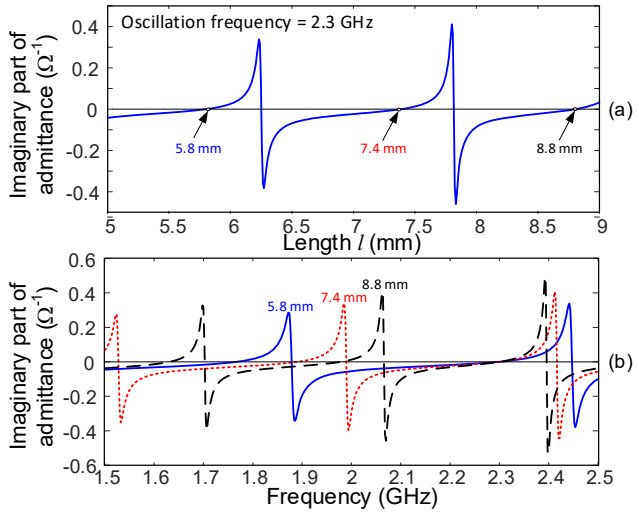

Fig. 2. Analysis of the slow-wave structure. (a) Susceptance at $\omega = \omega_o$ versus l to obtain the values fulfilling $B(l_n) = 0$. (b) Evaluation of $\partial B / \partial \omega$ at l_n.

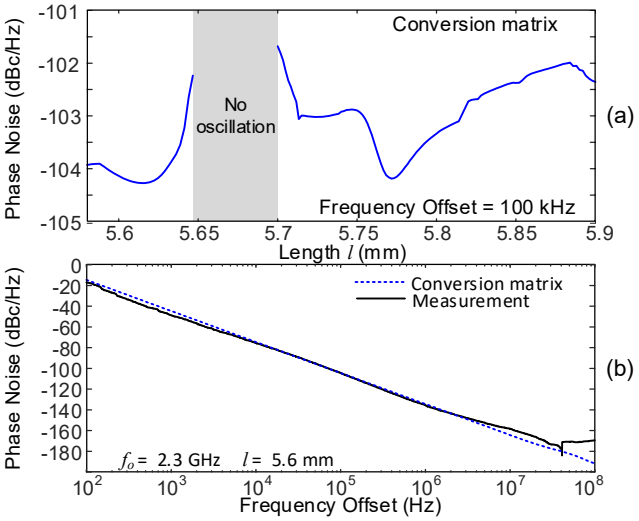

Fig. 3. Phase-noise minimization with an AG. (a) Phase noise at 100 kHz vs. l, when optimizing w and the AG amplitude to fulfill $Y_{AG}(A_{AG}, w) = 0$. (b) Phase-noise at l = 5.6 mm. Measurement with the R&S FSWP8 Phase Noise Analyzer.

The complete phase-noise spectrum is shown in Fig. 3(b), where it is compared with the experimental one, obtained with the R&S FSWP8 Phase Noise Analyzer. It is significantly lower than those obtained without the slow-wave structure in oscillators based on the same device (see the spectrum in [7] with -80 dBc at 100 kHz). Nevertheless, a higher spectra purity might be possible with other slow-wave structures.

III. Analytical Formulation

The analytical formulation of the SOM containing the slow-wave structure will be based on a simple model (Fig. 4). There are two fundamental frequencies: the oscillation frequency ω_o and the input frequency ω_1. The nonlinear *transconductance* current is:

$$i(t) = g_m v(t) + g_2 v(t)^2 + g_3 v(t)^3 \tag{1}$$

with $g_m > 0$, $g_3 < 0$. The voltage v and current i will be expressed in a Fourier basis at the frequencies ω_o, ω_1, $\omega_{IF} = \omega_1 - \omega_o$ and $\omega_s = \omega_1 + \omega_o$:

$$\begin{aligned} v(t) &= \mathrm{Re}\left\{V_o e^{j\omega_o t} + V_1 e^{j\omega_1 t} + V_{IF} e^{j\omega_{IF} t} + V_s e^{j\omega_s t}\right\}, \\ i(t) &= \mathrm{Re}\left\{I_o e^{j\omega_o t} + I_1 e^{j\omega_1 t} + I_{IF} e^{j\omega_{IF} t} + I_s e^{j\omega_s t}\right\} \end{aligned} \tag{2}$$

where due to the oscillator autonomy, the phase of V_o is arbitrarily set to zero. The frequency-domain system is:

$$\begin{aligned} &V_o + A_y(\omega_o) I_o = 0, \\ &V_1 + A_y(\omega_1) I_1 + A_g(\omega_1) E_{in} = 0, \\ &V_{IF} + A_y(\omega_{IF}) I_{IF} = 0 \\ &V_s + A_y(\omega_s) I_s = 0 \end{aligned} \tag{3}$$

where A_y and A_g are frequency-dependent functions accounting for the passive linear network (and thus, including the effect of the slow-wave structure). For the simple model of Fig 4:

$$\begin{aligned} &A_y(\omega) = Z_{gs} Z_s / den, \\ &A_g(\omega) = -\left[1 + Y_{ds}\left(Z_s + Z_{out}\right)\right] Z_{gs} / den, \\ &den = Z_g + Z_{gs} + Z_s + Y_{ds}\left[(Z_{out} + Z_s)(Z_g + Z_{gs}) + Z_s Z_{out}\right] \end{aligned} \tag{4}$$

And the expressions of I_o, I_1 and I_{IF} are:

$$\begin{aligned} I_{IF} &= g_m V_{IF} + g_2 V_1 V_o + g_3 \left(\frac{3V_1^2 V_s^*}{4} + \frac{3V_o^2 V_s}{4} + \frac{3V_{IF}\left(V_o^2 + |V_1|^2\right)}{2} \right) \\ I_o &= g_m V_o + g_2\left(V_1^* V_s + V_{IF}^* V_1\right) + g_3\left(\frac{3V_o |V_1|^2}{2} + \frac{3V_o^3}{4} \right) \\ I_1 &= g_m V_1 + g_2 V_o\left(V_s + V_{IF}\right) + g_3 \frac{3|V_1|^2 V_1}{4} \end{aligned} \tag{5}$$

where some low amplitude terms have been neglected. For small E_{in}, I_o will be real since V_s and V_{IF} will be negligible. Thus, the oscillation frequency is determined by $\mathrm{Im}[A_y(\omega_o)] = 0$. Assuming for simplicity $Y_{ds} \cong 0$, $Z_{gs} = jX_{gs}$ and $Z_s = jX_s$, and splitting the equation at ω_o into real and imaginary parts:

$$\frac{-R_g}{X_{gs} X_s} + \frac{I_o(V_o, |V_1|)}{V_o} = 0, \quad B_s + \frac{1}{X_g + X_{gs}} = 0 \tag{6}$$

Due to the high slope of B_s (Section II), the ω_o value resulting from the second equation will be very close to the resonance frequency of the slow-wave structure. When E_{in} increases, I_{IF} will increase too and, from (3)-(5), the complex term

$g_2(V_1^* V_s + V_{IF}^* V_1)$ $g_2 V_{IF}^* V_1$ of I_o [see (4)] will give rise to a deviation of the oscillation frequency ω_o from the one predicted from $\mathrm{Im}[A_y(\omega_o)] = 0$. This will lead to an undesired dependence of the IF frequency on the input power P_{in}. However, in the presence of the slow-wave structure this frequency variation should be limited.

For small E_{in}, we can approach $V_1 \cong -A_g(\omega_1)E_{in}/[1+A_y(\omega_1)]$. Then, under the reasonable assumption of a small IF current through Y_{ds}, the linear conversion gain (G_c) is:

$$G_c = 4R_o\,\mathrm{Re}\left[Z_{out}(\omega_{IF})\right]\left|I_{IF}\right|^2 / E_{in}^2 \cong$$
$$G_c = 4R_o\,\mathrm{Re}\left[Z_{out}(\omega_{IF})\right]\left|A_g(\omega_1)\right|^2 \left|g_2 V_o\right|^2 / \left|1+A_y(\omega_1)\right|^2 \quad (7)$$

The terms $A_g(\omega_1)$ and $A_y(\omega_1)$ will have an impact on G_c, so the effects of Z_{gs} and Z_s should be compensated for a flat gain.

When increasing E_{in}, the gain will vary as:

$$G_c = \frac{4R_o\,\mathrm{Re}\left[Z_{out}(\omega_{IF})\right]}{E_{in}^{\,2}} \times$$
$$\left| g_m V_{IF} + g_2 V_1 V_o + g_3 \left(\frac{3V_1^2 V_s^*}{4} + \frac{3V_o^{\,2} V_s}{4} + \frac{3V_{IF}\left(V_o^{\,2} + |V_1|^2\right)}{2} \right) \right|^2 \quad (8)$$

As gathered from (4), from certain P_{in}, the oscillation amplitude V_o will decay due to the increase in $|V_1|$ [Fig. 5(a)]. However, this amplitude has not significantly decreased at the 1 dB compression point. In fact, there are two mechanisms for gain compression: the decrease of V_o in $g_2 V_o V_1$ and the growth in magnitude of the negative term in (8), which can be written in a compact manner as $g_3 f(V_o, V_1, V_{IF}, V_s)$. The second effect will lead to compression at a lower P_{in} for a higher small-signal conversion gain (giving larger $|V_{IF}|$ and $|V_s|$). Fig. 5(b) presents the evolution of G_c, as well as the magnitudes of the second and third terms in (8) versus P_{in}. The magnitude of the third term experiences a quicker growth near the compression point.

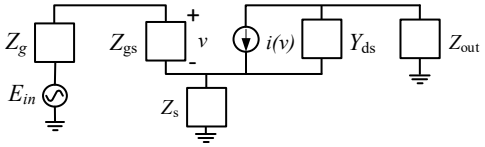

Fig. 4. Simple SOM model. The nonlinear transconductance current is $i(v)$, where v is the control-voltage waveform. For convenience, the blocks are expressed in terms of the immittances used in the mathematical derivations.

As P_{in} continues to increase, the growth of $|V_1|$ will give rise to a significant reduction of both V_o and $|V_{IF}|$, which will become zero at an inverse Hopf bifurcation [9] [Fig. 5(b)]. For each ω_1, this Hopf bifurcation is obtained by solving the following system in terms of $E_{in,H}$, $V_{1,H}$ and $\omega_{o,H}$.

$$V_{1H} + A_y(\omega_1)\left(g_m V_{1,H} + g_3 \frac{3}{4} V_{1,H} \left|V_{1,H}\right|^2 \right) + A_g(\omega_1) E_{in,H} = 0$$
$$1 + A_y(\omega_{o,H})\left(g_m + g_3 \frac{3}{2} \left|V_{1,H}\right|^2 \right) = 0$$

Under the nonlinear transconductance (1), the oscillation frequency is obtained from $\mathrm{Im}[A_y(\omega_o)] = 0$ and $E_{in,H}$ is:

$$E_{in,H} = \left| 1 + A_y(\omega_1)\left[g_m + g_3 \frac{3}{4} \left|V_{1,H}\right|^2 \right] \right| \left|V_{1,H}\right| / \left|A_g(\omega_1)\right|$$
$$\left|V_{1,H}\right|^2 = 2\left(-\left[\mathrm{Re}\, A_y(\omega_{o,H}) \right]^{-1} - g_m \right) / (3g_3) \quad (9)$$

$E_{in,H}$ increases with g_m and decreases with g_3 and $A_g(\omega_1)$.

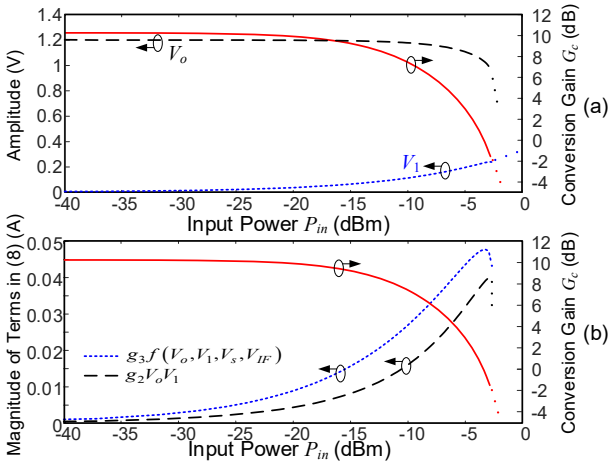

Fig. 5. Mechanism for the gain compression. (a) G_c and amplitudes V_1 and V_o vs. P_{in}. (b) G_c and magnitude of the second and third terms of (8) versus P_{in}.

IV. Practical SOM Design

The proof-of-concept SOM is based on the PHEMT ATF-34143 (Fig. 1). The bias point is V_{GS} = -0.5 V and V_{DS} = 2 V, with a consumption of 16 mW. Initially, we have performed a HB analysis of the small signal conversion gain versus the IF frequency. As seen in Fig. 6, positive gain is obtained above and below the free-running frequency. About this frequency, there is a narrow region with no heterodyne gain because of the DC feeds. Moreover, within this region the oscillation will get locked by the input source. Fig. 7(a) presents the variation of G_c for two different values of the input frequency with measurements superimposed. In consistency with the analytical study, the gain compression occurs at smaller input power for a larger small-signal gain. Fig. 7(b) presents the deviation of the oscillation frequency (vs. P_{in}) with respect to the free-running value, greatly reduced by the slow-wave structure and Fig. 7(c), the third-order intermodulation distortion. The discrepancies with respect to the simulation results are attributed to modelling inaccuracies.

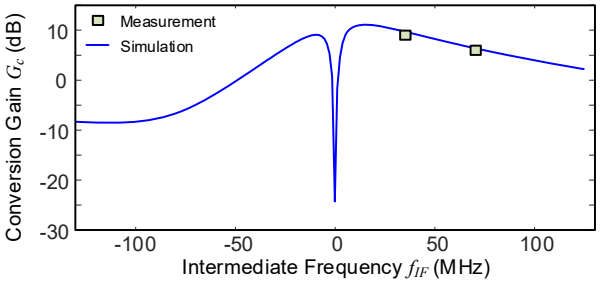

Fig. 6. Small-signal conversion gain versus the intermediate frequency.

For an exhaustive calculation of the inverse Hopf bifurcations (providing the SOM operation boundaries), a small-signal AG (which plays the role of the oscillation),

operating at ω_o, is introduced into the circuit. In this case, the AG is connected in parallel at the gate terminal. For each ω_{in}, a double sweep is carried out in the E_{in} and ω_o, evaluating the AG small-signal admittance at each sweep step. This provides the function $Y(\omega_{in}, P_{in}, \omega_o)$, which will be zero at the (ω_{in}, P_{in}) values where the oscillation is extinguished. The set of these bifurcations is detected by exporting the function $Y(\omega_{in}, P_{in}, \omega_o)$ and calculating its roots from the intersection of the zero-value contours of its real and imaginary parts. This method does not require any optimization of the AG and for each P_{in} or ω_{in}, it provides all the coexisting secondary Hopf bifurcations in an exhaustive manner. The results are shown in Fig. 8, with measurements superimposed. The Hopf locus has two sections, above and below the oscillation frequency in free-running conditions ω_o.

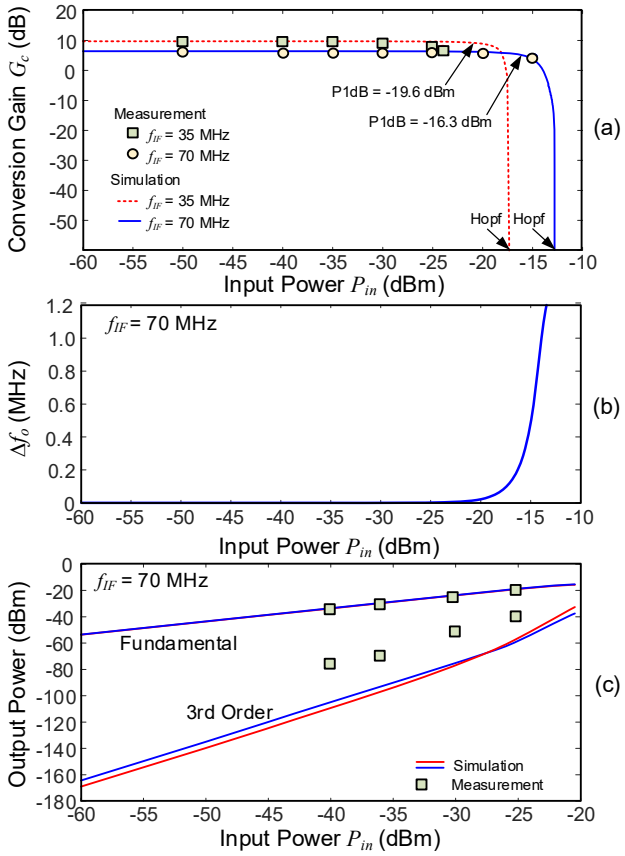

Fig. 7. (a) Gain variation versus P_{in} for two different IF frequencies. (b) Variation of the oscillation frequency. (c) Third order intermodulation.

When moving towards the locking region (from a quasi-periodic regime), the oscillation frequency ω_o progressively approaches ω_{in} and the two become equal at a local-global saddle node bifurcation [9], which geometrically corresponds to a turning point of the periodic solution curve. At the fundamental frequency of the locked/periodic solution, one has:

$$Y_{AG} A_{AG} - F_N \, E_{in} e^{j\phi} = 0 \qquad (10)$$

where ϕ is the opposite of the phase shift between the AG-node voltage and E_{in}, and F_N is a linear and frequency-dependent function. Note that the HB system constitutes the inner tier of (10). At any turning point, the Jacobian matrix of (10) with respect to A_{AG} and ϕ will be singular. The locking saddle-node bifurcations constitute a subset of these points, which, as easily derived, can be obtained from the condition:

$$\partial \left| Y_{AG} V_{AG} \right| / \partial V_{AG} = 0 \qquad (11)$$

The locus provided by (11) (Fig. 8) includes locking points (up to the merging with the Hopf locus) and turning points of the periodic solution curves (after the oscillation extinction). The locking region is very narrow (due to the high quality factor of the slow-wave structure), as confirmed in the experimental characterization.

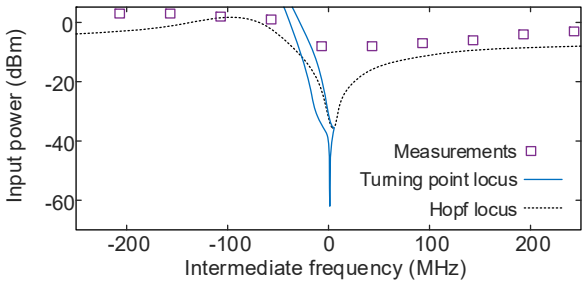

Fig. 8 Operation boundaries of the SOM, determined by bifurcation phenomena.

V. Conclusion

A self-oscillating mixer based on the use of a slow-wave structure for phase-noise reduction has been presented, together with an insightful analytical model and some new analysis methods for an optimum design.

Acknowledgement

This work was supported by the Spanish Ministry of Science and Innovation (MCIN/ AEI /10.13039/501100011033) under grant PID2020-116569RB-C31.

References

[1] C. E. Saavedra, B. R. Jackson and S. S. K. Ho, "Self-Oscillating Mixers: A Natural Fit for Active Antennas," *IEEE Microw. Mag.*, vol. 14, no. 6, pp. 40-49, Sept.-Oct. 2013.

[2] P. Burasa, B. Mnasri and K. Wu, "Millimeter-Wave CMOS Sourceless Receiver Architecture for 5G-Served Ultra-Low-Power Sensing and Communication Systems," *IEEE Trans. Microw. Theory Techn.*, vol. 67, no. 5, pp. 1688-1696, May 2019.

[3] M. Pontón, A. Herrera and A. Suárez, "Double Functionality Concurrent Dual-Band Self-Oscillating Mixer," *IEEE Trans. Microw. Theory Techn*, vol. 69, no. 1, pp. 786-802, Jan. 2021.

[4] V. Rizzoli, F. Mastri and D. Masotti, "General noise analysis of nonlinear microwave circuits by the piecewise harmonic balance technique," *IEEE Trans. Microw. Theory Techn*, vol. 42, no. 5, pp. 807–819, May, 1994.

[5] C. Zhou, H. Y. D. Yang, "Design Considerations of Miniaturized Least Dispersive Periodic Slow-Wave Structures," *IEEE Trans. Microw. Theory Techn.*, vol. 56, no. 2, pp. 467-474, Feb. 2008.

[6] A. K. Poddar, U. L. Rohde, "Slow-Wave Evanescent-Mode coupled resonator oscillator circuits," *IEEE Int. Frequency Control Symp. Proc.*, Baltimore, MD, 2012, pp. 1-7.

[7] M. Pontón, F. Ramírez, A. Herrera and A. Suarez, "Oscillator Stabilization Through Feedback With Slow Wave Structures," *IEEE Trans. Microw. Theory Techn*, vol. 68, no. 6, pp. 2358-2373, June 2020

[8] A. Suárez, *Analysis and Design of Autonomous Microwave Circuits*. Hoboken, NJ: Wiley IEEE Pres, 2009.

[9] J. Guckenheimer, P. J. Holmes, *Nonlinear Oscillations, Dynamical Systems, and Bifurcations of Vector Fields*, Springer, New York 1983.